Geomorphology 295 (2017) 323–336

Contents lists available at ScienceDirect

Geomorphology

journal homepage: www.elsevier.com/locate/geomorph

Yellow River terrace sequences of the Gonghe–Guide section in the northeastern Qinghai–Tibet: Implications for plateau uplift

Liyun Jia[a], Daogong Hu[a,*], Huanhuan Wu[a], Xitao Zhao[b], Pengyuan Chang[c], Baojie You[c], Meng Zhang[c], Chaoqun Wang[a], Mengni Ye[c], Zequn Wu[c], Xingzhong Liang[d]

[a] Institute of Geomechanics, Chinese Academy of Geological Sciences, Beijing 100081, China
[b] Institute of Geology and Geophysics, Chinese Academy of Sciences, Beijing 100029, China
[c] School of Earth Sciences and Resources, China University of Geosciences, Beijing 100083, China
[d] Department of Nuclear Material and Technology, Cheugdu University of Science and Engineering, Cheugdu 610059, China

ARTICLE INFO

Keywords:
Tibetan Plateau
Uplift
Yellow River
River terrace

ABSTRACT

The uplift of the Tibetan Plateau was a significant event in terms of global landforms and climate, but the exact nature of the uplift process remains contested among geologists. In the uplifted inland area of the plateau, river-terrace formation has been controlled mainly by tectonic uplift, which means that analyses of river terraces are an excellent means of investigating the uplift process. In this paper, we establish the terrace sequence of the Yellow River in the Gonghe–Guide section of the northeastern Tibetan Plateau, making use of field investigations, gravel analysis, and electron spin resonance (ESR) dating. Terraces T3–T9 of the numbered sequence formed at ~0.13, 0.18, 0.23, 0.41, 0.85, 0.93, and 1.32 Ma, (moving backwards in time and upwards from the valley floor), whereas terraces T11–T20 formed at ~1.71, 1.75, 1.88, 1.94, 2.01, 2.12, 2.23, 2.31, 2.36, and 2.47 Ma. This suggests that the Yellow River existed in Gonghe and Guide basins for at least the last 2.47 Ma. The incision rates of the Yellow River in the Gonghe–Guide section indicate that there were three distinct phases of uplift of the northeastern Tibetan Plateau, occurring at different rates, with an average uplift rate of ~0.26 mm/yr during the Quaternary. These results support the multi-stage uplift model, which states that the Tibetan Plateau has experienced continuous uplift since 8 Ma, but contradicts both the early uplift theory, which holds that the uplift of the Tibetan Plateau occurred mainly before the Pliocene, and the notion of a late and rapid uplift of the plateau that began at 3.6 Ma.

1. Introduction

Previous studies have sought to determine when the Tibetan Plateau reached its present elevation, and to calculate the uplift amounts and rates over time. The early uplift model holds that the uplift of the Tibetan Plateau occurred mainly before the Pliocene; e.g., Harrison et al. (1992) proposed that the plateau approached its current elevation at about 8 Ma, since then there has been little or no uplift. Others have proposed that the plateau reached its highest elevation in central part but that plateau outgrowth occurred at the same time about 14 Ma, and then subsided due to gravitational collapse (Molnar et al., 1993; Coleman and Hodges, 1995). Alternatively, those supporting a later uplift have proposed that the rapid uplift of Tibetan Plateau began at 3.6 Ma and has continued to the present day (Xu et al., 1973; Li et al., 1979, 2001; Li and Fang, 1999; Song et al., 2003). Other scholars believe that the uplift of the Tibetan Plateau is a multi-phase process that has progressed at different rates and over irregular intervals (e.g., Li, 1995; Zhong and Ding, 1996; Song et al., 2000; Tapponnier et al., 2001; Wang et al., 2008, 2012, 2014a). However, the exact uplift rate and amplitude since the late Cenozoic remain to be clarified.

River terraces are an important archives of past river activity, and they develop as a result of the accumulation of sediments and channel incision at various times. The factors that drive these processes consist primarily of changes of the internal dynamics of the fluvial system and controls that are external to the fluvial system. The latter include climatic, tectonic, and base-level changes (e.g., Merritts et al., 1994; Vandenberghe, 1995, 2002, 2003; Bridgland, 2000; Maddy et al., 2001a, 2001b, 2008; Vandenberghe and Maddy, 2001; Bridgland et al., 2004; Bridgland and Westaway, 2008; Westaway, 2009; Jia et al., 2016). In the inland uplift area of the Tibetan Plateau, fluvial terrace development has been driven by climate change and tectonic uplift. Tectonic uplift controls the depth of potential river downcutting, and climate controls the cyclicity in the aggradation of terraces, which are also affected by channel incision (e.g., Maddy et al., 2000; Bridgland

* Corresponding author.
E-mail address: hudaogong6699@126.com (D. Hu).

http://dx.doi.org/10.1016/j.geomorph.2017.06.007
Received 14 October 2016; Received in revised form 7 June 2017; Accepted 7 June 2017
Available online 02 July 2017
0169-555X/

et al., 2004; Bridgland and Westaway, 2008; Westaway, 2009; Wang et al., 2010; Herfried et al., 2012; Hu et al., 2012; Viveen et al., 2013; Ren et al., 2014; Jia et al., 2015, 2016). The rate of fluvial incision over long periods can reflect the conditions of tectonic uplift in tectonically active regions. This relationship has gained widespread acceptance over recent decades, based on the assumption that rivers should attain approximately their equilibrium gradient (e.g., Bridgland, 2000; Maddy et al., 2001a, 2008; Pan et al., 2009; Westaway, 2009; Vandenberghe et al., 2011; Jia, 2015; Vandenberghe, 2015).

The Yellow River flows through the Gonghe–Guide Basin, which is located between the Qilian and Kunlun mountains on the northeastern (NE) Tibetan Plateau. There are several well-developed river terraces in the basin that have the potential to provide reliable records of the uplift of the plateau, and these terraces have been the subject of several studies. For example, Miao et al. (2012) obtained ages for deposition of the T1 (0.017 Ma), T2 (0.043 Ma), and T4 (0.081 Ma) Yellow River terraces in the Guide reach. In addition, Perrineau et al. (2011) used ^{10}Be and ^{26}Al cosmogenic isotope dating to infer that the ongoing phase of Yellow River incision began at about 120–250 ka. However, lithostratigraphic research has demonstrated that plateau uplift began in the Oligocene (Zhang et al., 2008, 2010), and the magnetostratigraphic age of the end of the paleolake deposits (the lakes that once occupied the basins before the fluvial drainage) is 1.8 Ma, which could be taken as the approximate age of the development of the Yellow River in the basin (Nie et al., 2003). In addition, the Huangshui River, which runs across the NE Tibetan Plateau, has developed 11 levels of river terraces, and the ages of the highest terrace (T11) is within the range 11–14 Ma (Lu et al., 2004; Wang et al., 2014b). These findings show that the Yellow River may have been vertically incising its valley since the late Miocene or Pliocene, rather than from the late Pleistocene, as was previously thought (Perrineau et al., 2011; Miao et al., 2012; Wang et al., 2012, 2014a).

In this paper, we use field investigation, analyses of river gravels, and electron spin resonance (ESR) dating to establish the terrace sequence of the Gonghe–Guide section of the Yellow River of the NE Tibetan Plateau and to investigate the genesis of these river terraces. We also estimate the uplift rate of the NE Tibetan Plateau since 2.47 Ma, and consider the implications of these results, in the context of previous research, for the mode of uplift of the Tibetan Plateau.

2. Geological and geomorphological setting

Our study area covers the Gonghe and Guide basins, which are located on the NE Tibetan Plateau and are two of the important basins through which the Yellow River flows. The Gonghe Basin is about 280 km long and lies at an average elevation of 3070 m above sea level. The Guide Basin is at 2100–2300 m above sea level. These basins are surrounded by mountains that contain faults and folded rocks (Fig. 1). To the north of the area is Mount Qinghainan, to the southwest is Mount Ela and to the south and east are Mount Baji and Mount Zhamagari, which are part of the East Kunlun Range (Fig. 1).

Since the collision between the Indian and the Eurasian plates in the Eocene, the Tibetan Plateau has experienced a period of rapid uplift (e.g., Patriat and Achache, 1984; Dai et al., 2006; Royden et al., 2008; Wang et al., 2008). The northeastern margin of the Tibetan Plateau is underlain by Asian lithosphere and was uplifted by the thrusting and crustal thickening associated with movement along large, left-lateral strike-slip fault complexes (Molnar and Tapponnier, 1975; Fothergill and Ma, 1999). These splay faults can be traced for hundreds of kilometres as a series of southeast-trending elongate mountain ranges, which include the Qilian Mountains, Mount Riyue and Mount Qinghainan (Fig. 1). The activity of these faults is closely related to the geography pattern of basin-mountain tectonics (including the Gonghe–Guide basins), and the incision of the Yellow River.

The basal strata in this area are Proterozoic and Triassic rocks that are unconformably overlain by thick Cenozoic deposits. The extensively developed glutenite (sandy conglomerate) of the Gonehe Group (according to previous studies, the age of Gonghe Group is approximately early Pleistocene, but in fact, it might be older) is an important marker stratum here, and frequently serves as the bedrock to the river terraces.

3. Methods

3.1. Geological survey and measurement of terrace sections

To investigate the development of the Yellow River terraces, we completed a detailed geological field survey of four representative sections of the river (Fig. 1). Profiles 1 (P1) and 2 (P2) are located in the Guide Basin near the Songbaxia and Huangheqing bridges, respectively. Profile 3 (P3), the Wenchanggong section, is located at the western margin of the Guide Basin. Profile 4 (P4), the Longyangxia reservoir section, is located at the junction between the Gonghe and Guide basins. The terrace elevations were measured using a high-resolution global positioning system (differential GPS) and the terrace widths were measured using a laser range finder.

3.2. Gravel analysis

There are two high-level terraces in the Longyangxia reservoir section, with average elevations of 2930 and 3100 m. There remains debate over whether these two high terraces are Yellow River terraces (Xu et al., 1984; Zhao and Liu, 2005; Sun et al., 2007). To address this question, we analyzed the gravels at the top of the T20 “Santala” (3100 m) terrace, and the T19 “Ertala” terrace (2930 m). Fifty gravel clasts were randomly selected for analysis from an area of 2 m^2 in a section through the terrace sediments, and we recorded the roundness of the gravel (the A–E grades of roundness are well rounded, rounded, subrounded, subangular, and angular) and the lithology of the gravel.

3.3. Chronology

The base of the river terraces (i.e., the rock underlying the terraces) is composed of late Cenozoic fluvial–lacustrine sediments of the Gonehe Group, and previous research has shown that in this area the Yellow River developed at about 1.8 Ma (Nie et al., 2003). Therefore, we speculate that the river terrace deposits were deposited after the Pliocene. Optically stimulated luminescence (OSL) dating has become increasingly widely used in Quaternary research (Buylaert et al., 2007, 2008); however, because of the restricted timeframe to which OSL can be applied (ca. the last 50,000 yr), in this study we used ESR dating. The ESR dating method is used to measure the last exposure age of deposits containing quartz, and can date samples that are hundreds to millions of years old, which is far beyond the 50,000-yr limit of OSL dating (e.g., Grün, 1989a, 1989b; Chen et al., 1991; Liang, 1993; Gao and Liang, 1995; Laurent et al., 1998; Liang and Gao, 1999; Blackwell et al., 2016).

3.3.1. Sampling

Samples for ESR dating were collected from the sands of the Yellow River terraces, which are composed of well-rounded quartz. First, we removed the surface layer of weathered alluvium (to a depth of at least 50 cm) and ensured that the underlying sediments to be sampled were undisturbed and fresh. Then, a steel tube was driven into the fresh profiles, retrieved, and the ends immediately covered with black plastic. The tube nozzle was sealed with aluminum foil and wrapped with adhesive tape.

3.3.2. Testing

The sediment samples were transported to the Analysis and Testing Center at the Chengdu University of Technology, and the ESR dates were obtained following measurement of the E'center signals. To improve reliability, we used two methods to calculate the ESR dates: the

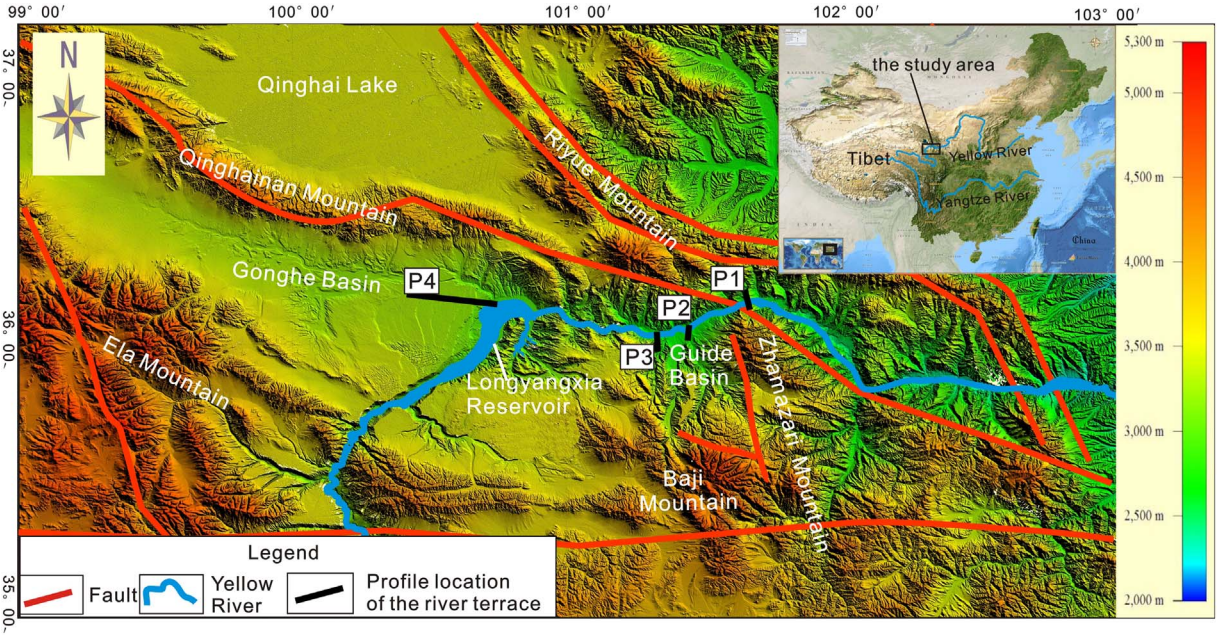

Fig. 1. Geomorphology and distribution of terraces in the study area. P1: Songbaxia section; P2: Huangheqing section; P3: Wenchanggong section P4: Longyangxia reservoir section.

artificial additive-dose technique and the heat-activated α quartz technique.

3.3.2.1. Artificial additive-dose technique. The artificial additive-dose technique is used to determine the natural accumulated ancient dose recorded in mineral grains (Grün, 1989a, 1989b). In practice, the natural accumulated dose is determined by exposing aliquots of the sample to artificial γ-radiation so that the specific ESR signal increases (Grün, 1989b; Liang, 1990, 1993; Liu et al., 2011). In this way, the ESR method can be used to date sediments of up to 1 Ma in age (Laurent et al., 1998), and it has been widely employed (e.g., Li and Fang, 1999; Beerten et al., 2006; Beerten and Stesmans, 2007; Pan et al., 2007; Rink et al., 2007).

The three fluvial sediment samples from the lower terrace (B1831-2, B1832-2, and B1819-1) were dated using the artificial additive-dose technique. In the laboratory, the samples were divided into two subsamples. The first was used to measure the concentrations of, and natural radioactivity generated by, the elements U, Th, and K. Approximately 500 g of this subsample was sealed in a Pb chamber for 15 d to allow measurement of the natural radioactivity levels. The U, Th, and K contents were measured using a CIT-3000F digital automatic U, Th, and K spectrometer, and the γ and α natural radioactivity was measured in the Pb chamber using an α spectral data acquisition system. This system was developed by the Chinese nuclear industry's Application Engineering Technology Research Center in the Nuclear Detection and Analysis Technology Research and Development Department. The second subsample was used to extract the quartz grains from the terrace sediments. The subsamples were washed in water and then sieved to obtain the 0.125–0.25 μm fraction, which was then treated with H_2O_2 to remove organic material and HCL to dissolve carbonate, and subsequently etched with concentrated HF for about 1 h to remove the outer layers of quartz grains. The samples were then washed thoroughly in water and allowed to dry naturally. Finally, the magnetic minerals in the samples were removed using a magnetic separator. Each sample was then divided into eight aliquots (ca. 120 mg each) and irradiated with a ^{60}Co source. The irradiated samples were then measured using a German ER-200D-SRC ESR spectrometer with the measurement conditions indicated in Table 1.

A typical ESR spectrum and a dose–response curve obtained from the quartz samples are shown in Fig. 2. The annual doses were calculated from the U, Th, and K contents (Aitken, 1985). The age of the sample (A) was calculated as A = P/D, where P is the paleodose and D is the annual dose.

Table 1
Measurement conditions of the irradiated samples.

Room temperature: 20–25 °C	Microwave frequency: 9.7652 GHz
Microwave power: 0.21–0.30 mW	Modulated amplitude: 0.25 Gpp
Modulation frequency: 100 kHz	Amplification coefficient: 7.11×10^5–1.26×10^6
Time constant: 50 ms	Scanning field range: 3462.5–3550.0 G
Central field: 3500.0 G	Magnetic field intensity: 3525.0–3527.5 G
Split spectra factor: g = 2.0005 ± 0.0005	Paramagnetic center density of the standard sample: 2.58×10^{15}/g

3.3.2.2. Heat-activated ESR dating of quartz. Previous experiments have shown that the artificial additive-dose approach to ESR dating is not suitable for samples for which > 1 Ma has elapsed since signal saturation (e.g., Chen et al., 1991; Liang, 1993; Liang and Gao, 1999). The heat-activated ESR dating of α quartz is based on the thermal activation processing of the samples, in which the E''_1 and E_{10} diamagnetic centers can be changed to the paramagnetic E'_1 center (Liang and Gao, 1999). As the total radiation energy of the paramagnetic and diamagnetic centers represents the total absorbed dose, we can determine the natural accumulated ancient dose of a quartz sample by measuring the ESR spectroscopy of the heat-activated sample. The experimental procedure for α quartz thermal activation does not require an artificial additive-dose, because the diamagnetic center is formed over long periods of geological time by low levels of irradiation. Two typical ESR spectra obtained from the quartz of the Yellow River terrace sediments are shown in Fig. 3. The maximum age for the heat-activated ESR dating of α quartz can reach 200 Ma, and this approach has been widely used in studies of faults and volcanoes (e.g., Zhong et al., 2004; Yang et al., 2006; Shen et al., 2008; Zhu et al., 2011; Ren et al., 2016). This method can also be used to test the sediment, but

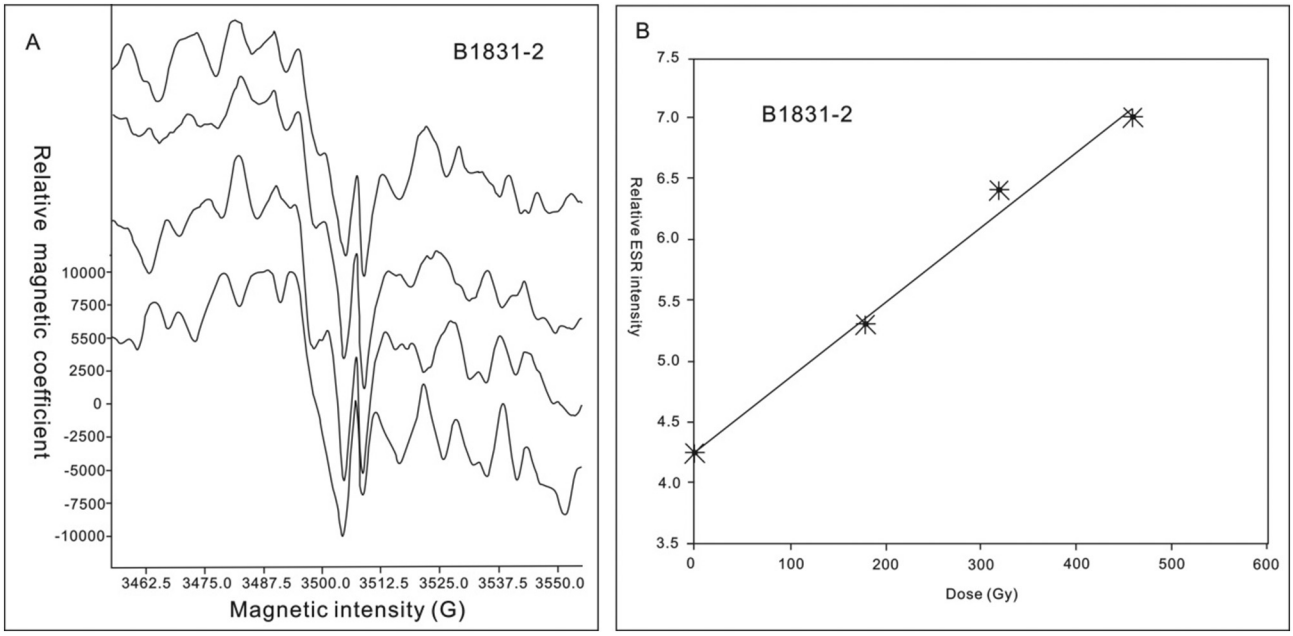

Fig. 2. A typical (A) ESR spectrum and (B) dose–response curve of ESR intensity for quartz grains from the terrace sediments of the Yellow River (from sample B1831-2).

the background values need to be deducted if the ESR intensity has not returned to zero. Our tests showed that most of the background values from this batch of samples had only a very small fluctuation. Consequently, we used the mean instead of the background value to generate the most reliable results. We tested these samples (except the three samples of B1831-2, B1832-2, and B1819-1) by the heat-activated α quartz technique. We determined the paramagnetic centers after the process of quartz heat activation. According to the ratio of the contents of U, Th, and K and the cosmic ray radiation dose, we translated the energy of Th, K and cosmic rays into the uranium equivalent, and obtained the α quartz age. For detailed information regarding the principles of ESR dating, see Grün (1989a, 1989b), Huang (1994), Liang (1993), and Liang and Gao (1999) and references therein.

4. Results

4.1. Section profiles of the Yellow River terraces

The geomorphological and sedimentary characteristics of the four terrace sections in the Gonghe and Guide basins are described below.

4.1.1. Songbaxia section (P1)

The Songbaxia section is located where the Yellow River flows out of the Guide Basin (Fig. 1), and we defined six Yellow River terraces at this site. Terraces T1, T2, T3, and T4 are all fill terraces, whereas Terraces T5 and T6 are strath terraces (Fig. 4). Terraces T1, T2, and T3, on the northern side of the river, have been reclaimed as farmland. The

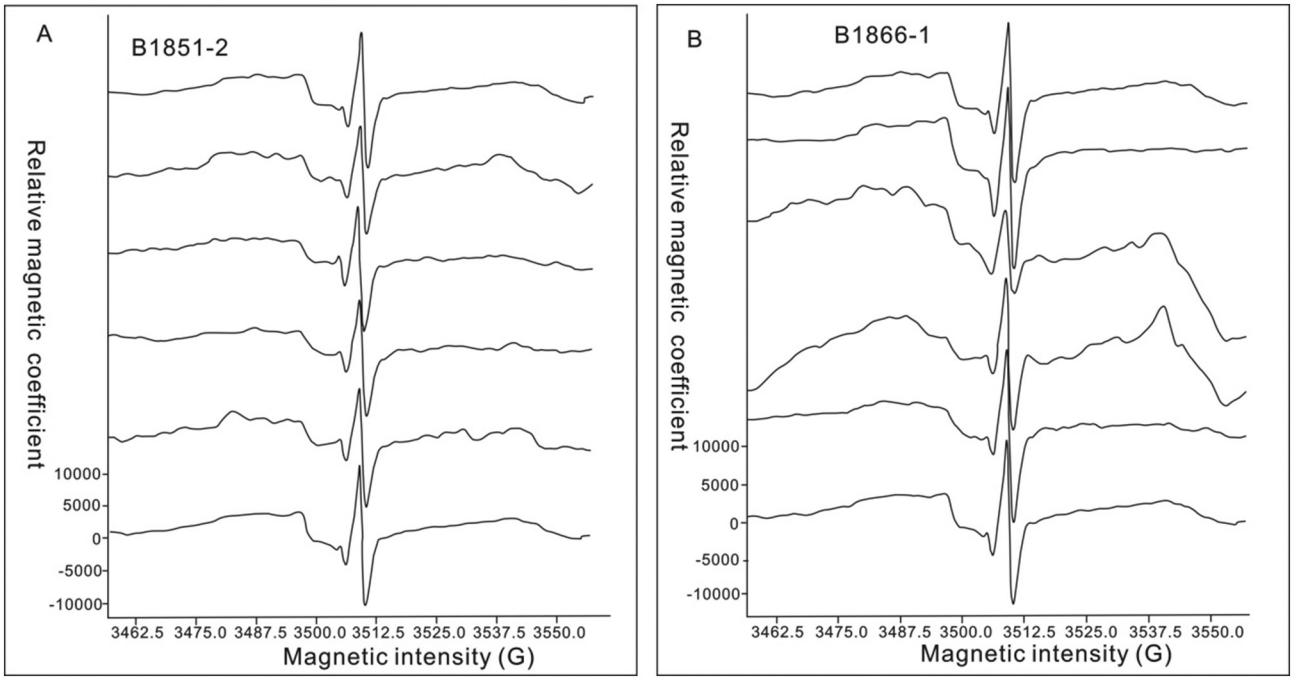

Fig. 3. Typical ESR Resonance spectra of quartz extracted from of B1851-2 and B1866-1 (heat-activated ESR dating of a quartz technique).

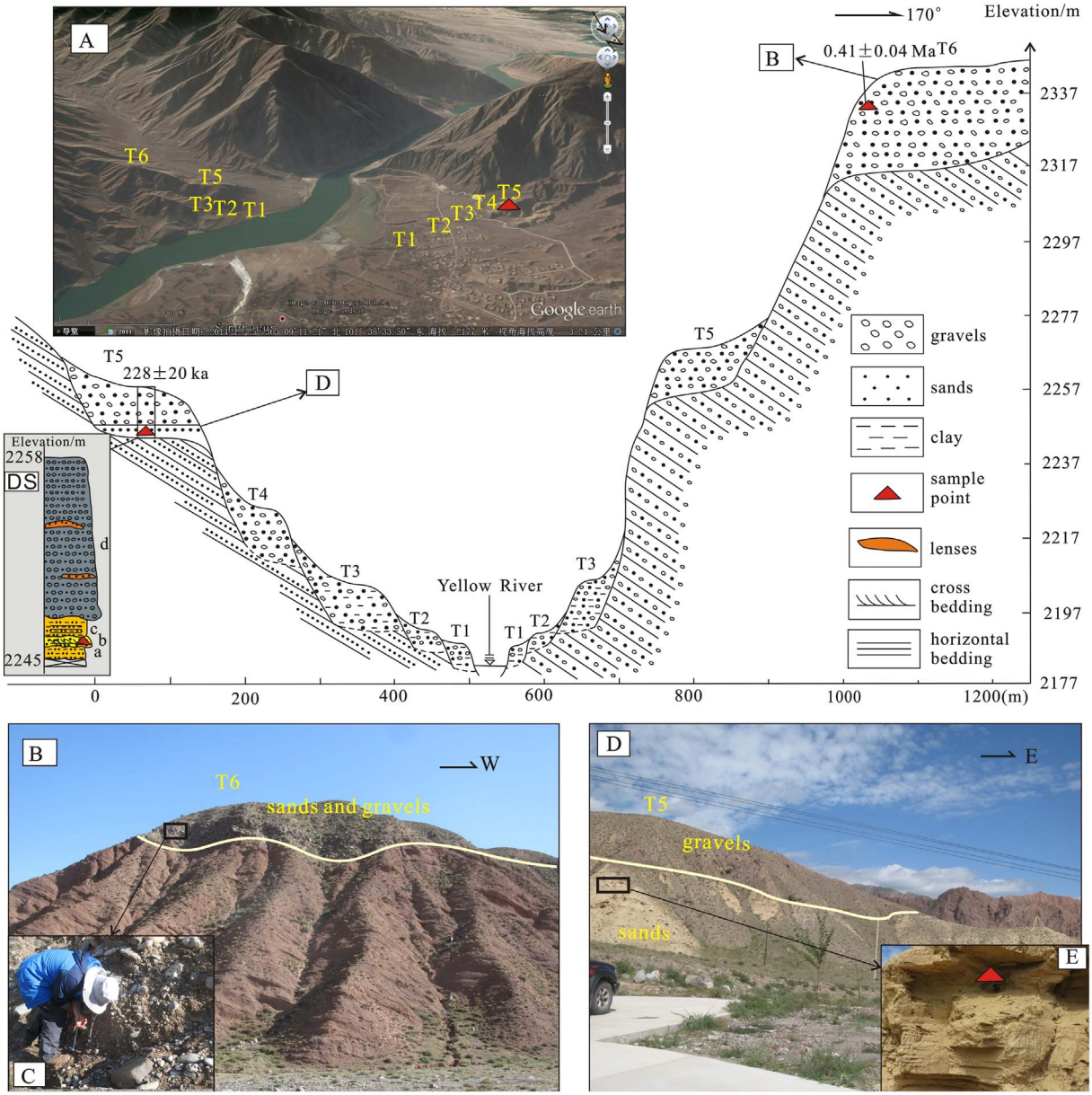

Fig. 4. Schematic profile of Yellow River terraces in the Songbaxia section (P1). (A) Google Earth image of river terraces in the Songbaxia section. (B–E): Outcrops of the T6 and T5 terraces and photographs of field sampling. (DS): (a) silty clay with fine sand interbedding; (b) coarse sand with cross bedding; (c) silty clay with horizontal bedding; (d) alluvial gravels with sand lenses, moderately rounded, sorting, and orientation; 3–16 cm in diameter, moderately weathered.

average heights of the terraces above the Yellow River are about 166 m (T6), 89 m (T5), 56 m (T4), 34.5 m (T3), 17 m (T2), and 11 m (T1), and the average thickness of every terrace is shown in Table 2.

4.1.2. Huangheqing section (P2)

The Huangheqing section is located in the northern Guide country town (Fig. 1). We identified four Yellow River terraces in this section, with the average heights above the Yellow River at about 70.5 m (T4), 35 m (T3), 20 m (T2), and 8 m (T1). The deposits that make up Terraces T4 and T3 are clayey silt with gravel silty sand. Terrace T2 sediment is a floodplain facies containing interbedded gravels and sands, and Terrace T1 is also composed of sand and gravel deposits, with well-bedded alluvial gravels showing medium roundness (Fig. 5).

4.1.3. Wenchanggong section (P3)

The Wenchanggong section is located at the western side of the Guide Basin, and five terraces were identified here (Fig. 6). The T1, T2, and T3 terraces are fill terraces, whereas theT4 and T6 terraces are base terraces (a type of strath terrace that is composed of river sediments overlying base bedrock, which means that river incision exceeds the terrace sediment thickness so that bedrock is exposed in the lower portion of the terrace scarp) in which the sediments are mainly sands and gravels. The gravels on the T6 terrace are well rounded, well sorted, and lithologically complex, with the clasts consisting of a mixture of quartzite, sandstone, granite, granite porphyry, vein quartz, metamorphic rocks, granodiorite, quartz sandstone, limestone, volcanic rocks, conglomerate, and mudstone.

4.1.4. Longyangxia reservoir section (P4)

The Longyangxia reservoir is located in the upper reaches of the Yellow River on the NE Tibetan Plateau and links the Gonghe Basin with the Guide Basin (Fig. 1). The 20 levels of Yellow River terraces are clearly visible to the northwest of the Longyangxia reservoir (Fig. 7). The elevation of the water surface is about 2575 m and the riverbed is at 2458 m. From the other sections at the Songbaxia, Huangheqing, and Wenchanggong profiles described above, we know that there are five to

Table 2
Survey data from Yellow River terraces in the Gonghe–Guide section.

Location	Terrace level	Height above the Yellow River (m)	Alluvium thickness (m)	Location	Terrace level	Height above the Yellow River (m)	Alluvium thickness (m)
Songbaxia section	T1	11–12	11–12	Longyangxia reservoir section	T7	165–172	10
	T2	14–20	2–8		T8	186–197	11
	T3	27–42	13–22		T9	210–220	15
	T4	48–64	21–22		T10	236–241	10
	T5	80–90	20		T11	249–258	14
	T6	165–167	30		T12	284–287	10
Huangheqing section	T1	6–8	6–8		T13	324–326	10
	T2	15–20	9–12		T14	327–335	20
	T3	30–40	15–20		T15	381–382	6
	T4	61–80	31–40		T16	396–405	15
Wenchanggong section	T1	6–11	6–11		T17	420–422	9
	T2	15–20	9		T18	446–482	12
	T3	30–40	15–20		T19	503–510	18–37
	T4	64–80	20		T20	643–648	10
	T6?	125–160	25				

Note: "?" means that the affinity to this terrace is uncertain.

six levels of river terraces located at < 100 m above the bed of the Yellow River. Previous studies have also reported river terraces lower than the reservoir surface (Xu et al., 1984; Zhao and Liu, 2005). From our comparison of the terrace heights above the Yellow River (T7 height of the Longyangxia reservoir section above the Yellow River bed is 172 m, and the T6 height of other sections are about 160 m) with the three profiles above, we infer that there should be six levels of river terraces submerged beneath the reservoir, based on the height difference of 117 m between the reservoir water surface and the bed of the Yellow River. Therefore, the first terrace above the Longyangxia reservoir water surface should be Terrace T7 of the Yellow River, with terraces T8–T20 above. The gravels on the terraces were well bedded and of medium roundness (Fig. 7; C1, C2, and C5).

Moreover, Xu et al. (1984) concluded that T18 is a Yellow River terrace, whereas T19 and T20 are both remnants of the former maximum accumulation surface (a paleosurface) of the Gonghe Basin. Therefore, we made a detailed investigation of the highest terrace in section P4, including its sedimentary and geomorphology characteristics. Our results show that the surfaces of terraces T18, T19, and T20 are very broad: T18 is about 3700 m wide, and T19 and T20 are about 8900 and 6500 m wide, respectively. In addition, the sediments of the three terraces show similar fluvial features (see Section 4.2).

4.2. Gravel analysis

From the results of our geological survey, we know that most of the fluvial gravels on the Yellow River terraces are complex, well sorted, and well rounded. To determine whether the gravels on terrace T19 and T20 are Yellow River sediments, which is disputed by some scholars (see section 4.1.4), we analyzed the gravels from the top of terraces T20 (3100 m) and T19 (2930 m).

On terrace T19, we randomly selected 50 clasts for analysis from an area of 2 m^2 at the front edge of the terrace. We found that 2% of the clasts are slightly weathered, 47% are moderately weathered, and 12%

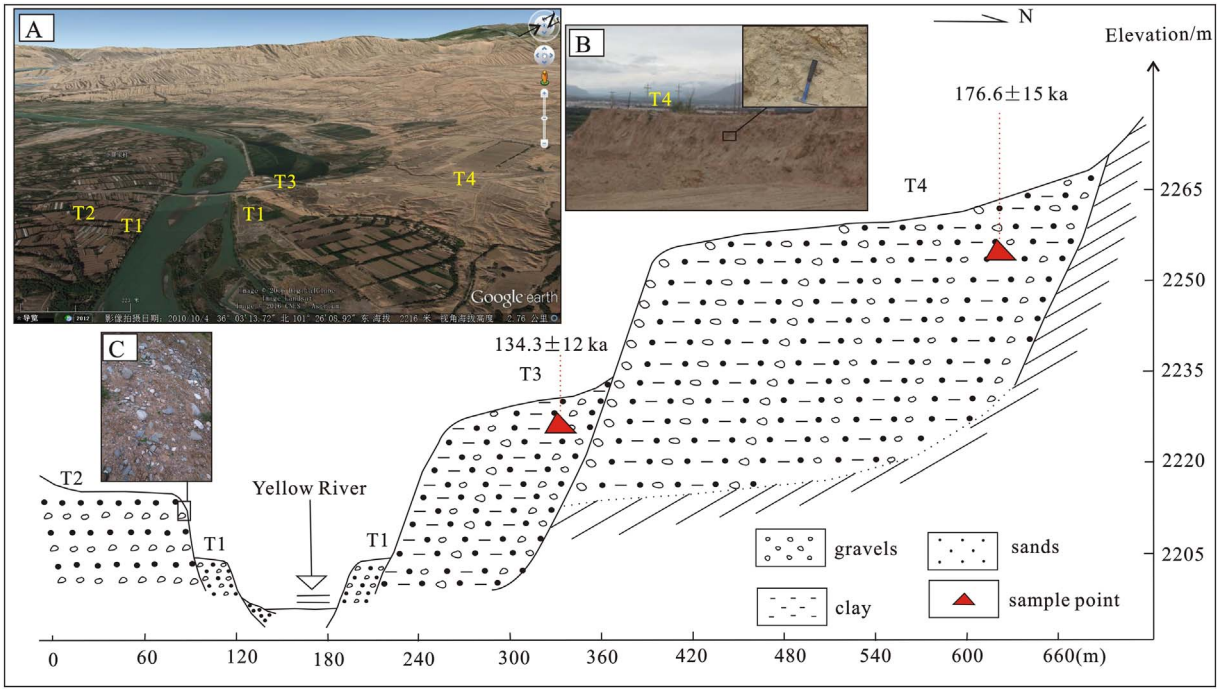

Fig. 5. Schematic profile of Yellow River terraces in the Huangheqing section (P2). (A) Google Earth image of the river terraces in the Huangheqing section. (B) Outcrop of T4 and photographs of field sampling. (C) Gravels on the T2 terrace.

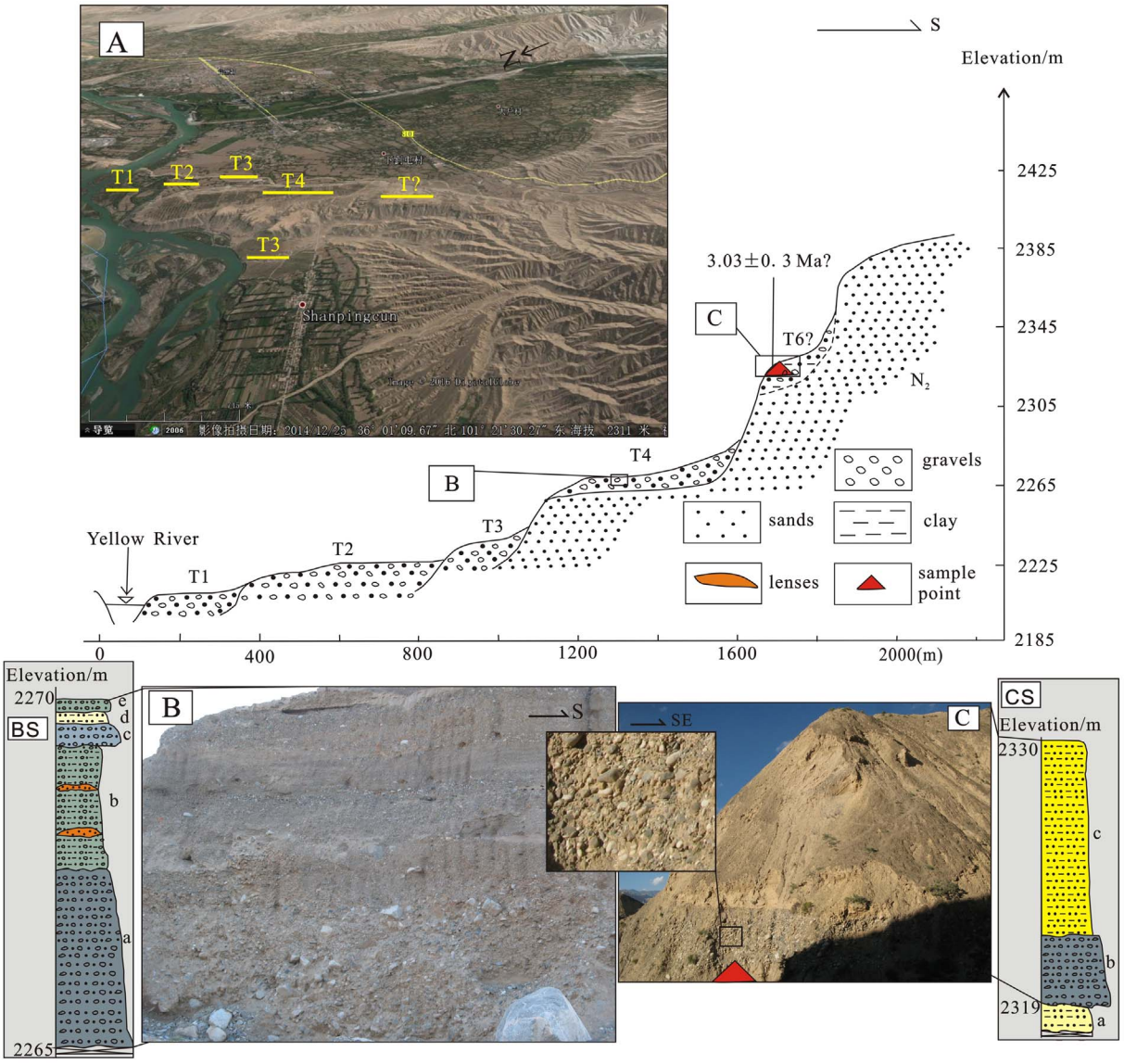

Fig. 6. Schematic profile of Yellow River terraces in the Wenchanggong section (P3). (A) Google Earth image of the river terraces in the Wenchanggong section. (B) Outcrop of T4 and photographs of field sampling. (C) Gravels on the T6? terrace. (BS): (a) alluvial-diluvial gravels, angular, poor sorting and orientation, 8–30 cm diameter; (b) alluvial-diluvial gravels with sand lenses, with a little clay, poor sorting and orientation, the gravels are about 1–7 cm in diameter; (c) alluvial-diluvial gravels, poor sorting and orientation, 1–15 cm in diameter; (d) silty clay with fine sand interbedding; (e) alluvial-diluvial gravels, poor sorting and orientation, 1–4 cm in diameter. CS: (a) silty clay; (b) alluvial gravels, moderately rounded, sorting, and orientation, 6–15 cm in diameter, moderately weathered; (c) silty clay with fine sand interbedding.

are highly weathered. The proportion of B (rounded) and C (sub-rounded) grade gravels is 86%, and the A (well rounded) and D (sub-angular) grade gravels account for the remaining 14% (Fig. 8). We identified 12 lithologies among the clasts: granite, sandstone, granite porphyry, vein quart, metamorphic rocks, granodiorite, quartzite, quartz sandstone, limestone, volcanic rocks, conglomerate, and mud-stone.

On terrace T20, we also found a layer of fluvial gravels (Fig. 7) that we analyzed. As shown in Fig. 9, the B and C grade gravels make up 80% of this terrace, and the A and D grade gravels make up 20%. Moderately weathered gravels account for 26% of the deposit (Fig. 9). This gravel is also lithologically mixed, and consists of similar rock types to those found on terrace T19 and listed above.

The lithological composition of the gravels on terraces T19 and T20 was almost the same, contain > 12 types of rocks, and some of the gravels cannot found locally (e.g., granite porphyry, quartz sandstone), so they must be brought here by a large river with a distant source (i.e., the Yellow River). Of course, the gravels on the T19 and T20 terraces not only came from the Yellow River, and some of them should have come from local sediments (contain the gravels of the tributaries and the planation surface), but the T19 and T20 terraces cannot be formed without the effect of the incision of the Yellow River, and most of the gravels are well rounded, and > 26% gravels are moderately weathered and highly weathered.

All of these data and phenomena show that the T19 and T20 terraces are Yellow River terraces (the gravel is lithologically mixed, and well rounded), and their age cannot be so young (as indicated by the high degree of weathering of the gravels).

4.3. Dating results and error analysis

4.3.1. Dating results

The two batches of ESR dating results are shown in Table 3 and Table 4. The ages of the Yellow River terraces fall entirely within the Quaternary, and the results are as expected, except for samples B1829-1 (from the “Wenchanggong” section) and B1843 (from the “Longyangxia

(caption on next page)

Fig. 7. Schematic profile of Yellow River terraces in the Longyangxia reservoir section (P4). (A) Digital elevation model of Yellow River terraces in the Longyangxia reservoir section. (B) Google Earth image of the lower terraces in the Longyangxia reservoir section. (C) Profile of Yellow River terraces in in the Longyangxia reservoir section. (C1–C6) Outcrop of terraces T19, T18, T16, T12, T10, and T7, respectively, and photographs of field sampling. (C1S): (a) alluvial gravels with sand lenses, moderate roundness, sorting, and orientation, 5–15 cm in diameter, moderately weathered; (b) clayey sand with horizontal bedding. (C2S): (a) alluvial gravels with sand lenses, moderate roundness, sorting, and orientation; 3–15 cm in diameter; (b) calcareous nodules; (c) loess. (C3S): (a) base sediments, medium-fine sands with horizontal bedding and cross bedding; (b) alluvial gravels with sand lenses, moderate roundness, sorting, and orientation; 4–12 cm in diameter; (C4S): (a) base sediments, medium-fine sands with horizontal bedding and cross bedding; (b) alluvial gravels with sand lenses, moderate roundness, sorting, and orientation; 5–15 cm in diameter, moderately weathered; (c) coarse sand with inclined bedding; (d) alluvial gravels, moderate roundness, sorting, and orientation; 2–13 cm in diameter. (C5S): (a) base sediments, medium-fine sands with horizontal bedding and cross bedding; (b) alluvial gravels with sand lenses, moderate roundness, sorting, and orientation; 1–8 cm in diameter.

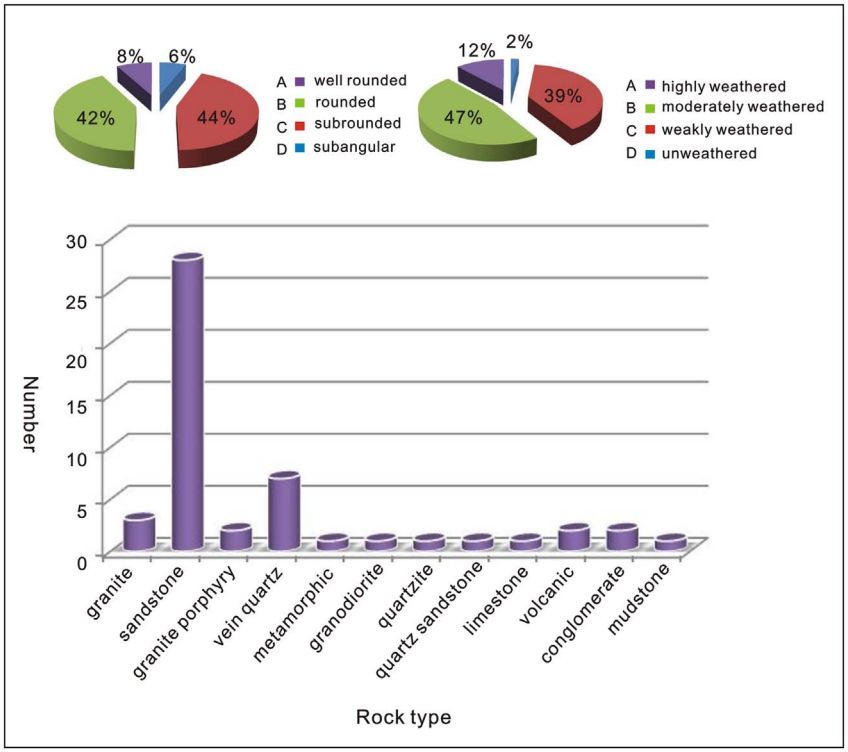

Fig. 8. Gravel composition, roundness, and degree of weathering for Terrace T19.

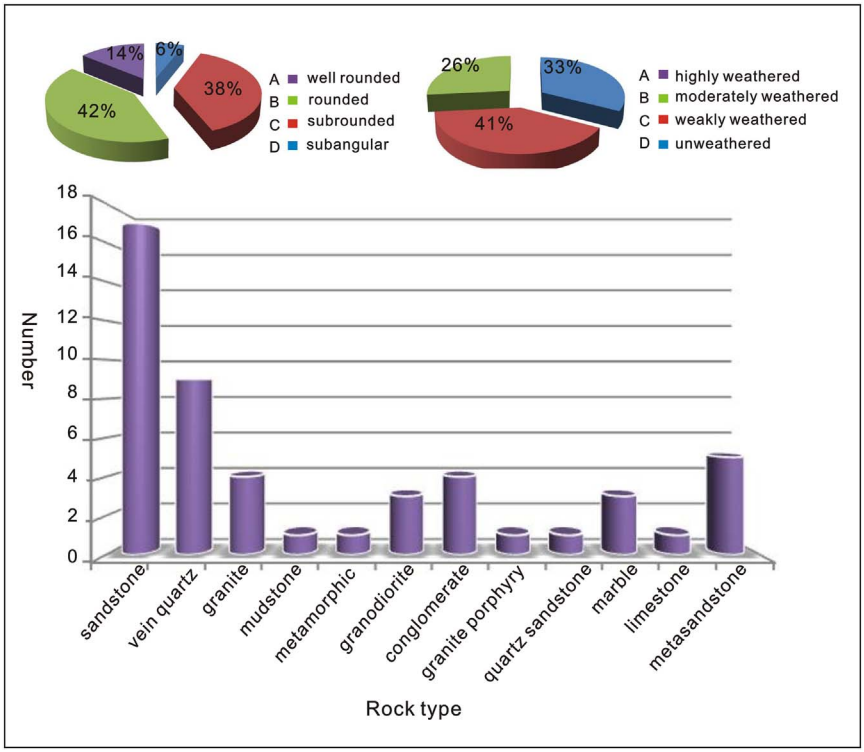

Fig. 9. Gravel composition, roundness, and degree of weathering for Terrace T20.

Table 3
Results of ESR dating for artificial additive-dose technique.

No.	Sample	Terrace level	Location	U (μg/g)	Th (μg/g)	K (%)	Paleodose (Gy)	Annual dose (mGy)	Age (ka)
1	B1831-2	T3(P2)	36°03′39.27″N, 101°27′11.77″E	1.20 ± 0.10	3.84 ± 0.30	2.12 ± 0.20	653.32 ± 39.20	4.86 ± 0.24	134.3 ± 12
2	B1832-2	T4(P2)	36°04′28.07″N, 101°26′43.23″E	2.02 ± 0.20	6.14 ± 0.60	2.10 ± 0.20	934.33 ± 48.50	5.29 ± 0.26	176.6 ± 15
3	B1819-1	T5(P1)	36°09′43.28″N, 101°38′15.4″E	2.21 ± 0.20	6.76 ± 0.65	1.76 ± 0.15	1533.33 ± 76.00	6.72 ± 0.33	228.1 ± 23

reservoir" section). The explanation for these unexpected results might be that these two samples were contaminated by other sediments.

4.3.2. Error and reliability analysis

The relative error associated with an ESR age is related to the experimental conditions. These errors can be introduced via statistical processing, natural radioactive decay of the elements U and Th, the standard used, instrumental error, etc. For the three samples B1831-2, B1832-2, and B1819-1, which were dated using the artificial additive-dose technique, the error of the paleodose was between 5% and 15%, and the error of the annual dose was < 5%, so that the total error associated with the absolute ages was 5–15%. For the heat-activated ESR dating technique, the total error is typically < 10% of the absolute age (Liang and Gao, 1999). The errors associated with the ESR spectrum amplitude measurement were < 1.7%, changes in the Th/U ratio were < 4.1%, and changes of the sealed U and Th decay were < 2.5%.

The results above show that the testing method adopted is feasible and the experimental results are reliable (most of the results are accord with the law of superposition or the regular of morphological evolution).

5. Discussion

5.1. Sequences and ages of Yellow River terraces in the Gonghe–Guide section

Theoretically, the ages of terrace sediments represent the time of deposition, whereas the ages of the uppermost beds can be regarded as the approximate time that the terrace was abandoned and incision to a lower level began (Jia et al., 2015). As our sampling sites are within the upper section of each terrace, the ESR ages of the terrace sediments (Tables 3, 4) can be regarded as the approximate formation time of the terraces. Therefore, the T3–T9 terraces formed at about 0.13, 0.18, 0.23, 0.41, 0.82, 0.93, and 1.32 Ma BP, and the T11–T20 terraces at about 1.71, 1.75, 1.88, 1.94, 2.01, 2.12, 2.23, 2.31, 2.36, and 2.47 Ma. BP, respectively (Table 5).

In previous research, Perrineau et al. (2011) designed seven levels in the vicinity of the Longyangxia section (P4) by remote sensing interpretation, without detailed field geological survey and measurement. Xu et al. (1984) designed 12 levels at the P4 section by field geological survey and measurement, but they failed to demonstrate that the T19 (Ertala) and T20 (Santala) terraces were formed by the Yellow River, as shown by the gravel analysis described above. They also omitted the six river terraces that we have shown to have been submerged in the Longyangxia reservoir. Thus, we have established 20 terrace levels of the Yellow River in the Gonghe-Guide section.

Moreover, previous research maintains that the Yellow River has only flowed through the Longyangxia section since 60 ka (after the Gonghe movement), and the ages of the Yellow River terraces in the Gonghe Basin should be late Pleistocene or younger (Yang and Wang, 1996). However, the Longyangxia gorge is developed in granite and volcanic rocks, and was incised to a depth of 800 m. If the Yellow River has only flowed in this reach since 60 ka, the implied rate of fluvial incision rate would reach 13.3 mm/yr, which is implausibly rapid. Therefore, our ESR ages (Tables 3 and 4), which imply that the Yellow River has existed in the Gonghe and Guide basins since 2.47 Ma, provides a considerably more reasonable interpretation.

5.2. Genesis of the Yellow River terraces in the Gonghe–Guide section

River terraces develop as a result of alternating cycles of sediment deposition and channel incision over time, and the factors that drive these processes are mainly changes in the internal dynamics of the fluvial system and external controls to the fluvial system, such as climatic, tectonic, and base level changes (e.g. Merritts et al., 1994; Vandenberghe, 1995, 2002, 2003, 2015, 2016; Bridgland, 2000; Maddy et al., 2001a, 2001b, 2008; Vandenberghe and Maddy, 2001; Bridgland et al., 2004; Bridgland and Westaway, 2008; Westaway, 2009). Intrinsic changes tend to occur over relatively short timescales (10–1000 yr) and produce small landforms (on a scale of 10–1000 m); such changes are caused by adjustments along individual reaches of a river (Maddy et al., 2001a, 2008; Vandenberghe, 2002).

In our earlier work, we studied the genesis of river terraces in inland uplifted areas and concluded that the sustained tectonic uplift controlled terrace development by providing the dynamic setting for river incision, and that climatic changes influenced the alternating cycles of incision and deposition caused by changes in the ratio of stream flow to sediment flux (Jia et al., 2015, 2016). The Yellow River terraces of the Gonghe–Guide section are located on the NE Tibetan Plateau, which is a typical area of inland uplift. Thus, the genesis of the 20 terrace levels here is expected to be the product of the combined action of tectonic uplift and climatic fluctuations, with the tectonic uplift controlling the height of the terraces by limiting the dissection depth and incision rate.

5.3. Incision rate of the Yellow River on the NE Tibetan Plateau and implications for plateau uplift

Although there is no simple theoretical relationship between fluvial incision and surface uplift (Whipple et al., 1999), it is widely accepted that the rate of fluvial incision over long periods can be used to quantify (or at least approximate) the rate of uplift in tectonically active regions (Bridgland, 2000; Maddy et al., 2001a, 2008; Dai et al., 2006; Martins et al., 2009; Pan et al., 2009; Westaway, 2009; Hu et al., 2012; He et al., 2014, 2015; Jia et al., 2015).

We used our dating results and the terrace elevation data to calculate the rates of river terrace incision in the study area. The highest Yellow River terrace in the Gonghe–Guide section is the T20 terrace, which has an average height above the riverbed of 643 m and an ESR age of about 2.47 Ma. Therefore, the average incision rate of the Yellow River during the Quaternary in the Gonghe–Guide Basin is approximately 0.26 mm/yr.

We also calculated the average incision rates at every stage, and the incision rates have fluctuated considerably over time (Fig. 10). Note that three main stages with different incision rates can be identified: from 2.47–1.71 Ma the average incision rate was ~0.51 mm/yr, from 1.71–0.41 Ma it was 0.09 mm/yr, and between 0.41 Ma and the present day it has increased to 0.35 mm/yr. However, the range of the average incision rate is relatively narrow, at ~0.15–0.39 mm/yr.

As discussed above, tectonic uplift is the main driving force of Yellow River downcutting in the research area; consequently, the incision rates can be used to constrain the history of tectonic uplift. Therefore, the incision rates of the Yellow River in the Gonghe–Guide section indicate that the uplift of the NE Tibetan Plateau proceeded in three different stages as defined by the incision rates. The average uplift rate since 2.47 Ma is ~0.26 mm/yr.

Table 4
Results of ESR dating for α quartz heat-activated technique.

No.	Sample	Terrace level	Location	U (μg/g)	Th (μg/g)	K (%)	Paramagnetic center concentration (10^{15} spin/g)	U equivalent	Age (Ma)
1	B1829-1	T6? (P3)	36°00′57.21″N, 101°21′26.66″E	4.00 ± 0.40	12.03 ± 1.20	2.82 ± 0.20	4.48	9.49 ± 0.56	3.03 ± 0.30
2	B1827-1	T6(P1)	36°00′51.06″N, 101°20′56.89″E	2.82 ± 0.25	8.58 ± 0.70	2.91 ± 0.20	4.56	7.47 ± 0.45	0.41 ± 0.04
3	B1828-1	T7(P4)	36°00′46.73″N, 101°20′45.30″E	3.36 ± 0.30	10.21 ± 1.00	2.72 ± 0.20	3.53	8.61 ± 0.43	0.85 ± 0.08
4	B1846-1	T7(P4)	36°09′36.73″N, 100°43′08.38″E	4.00 ± 0.40	12.03 ± 1.20	1.68 ± 0.15	3.50	4.79 ± 0.26	0.82 ± 0.08
5	B1847-1	T8(P4)	36°09′50.64″N, 100°42′52.17″E	3.79 ± 0.35	11.31 ± 1.00	1.71 ± 0.15	3.542	4.923 ± 0.24	0.93 ± 0.10
6	B1848-1	T9(P4)	36°09′59.11″N, 100°42′46.46″E	2.88 ± 0.28	8.77 ± 0.80	1.55 ± 0.15	3.39	3.51 ± 0.19	1.32 ± 0.10
7	B1843-2	T10(P4)	36°07′59.99″N, 100°41′07.42″E	3.36 ± 0.30	10.21 ± 1.00	1.62 ± 0.15	3.5	4.79 ± 0.28	2.20 ± 0.20
8	B1849-1	T11(P4)	36°10′30.30″N, 100°42′25.81″E	2.54 ± 0.25	7.80 ± 0.70	1.66 ± 0.15	3.99	3.34 ± 0.16	1.71 ± 0.13
9	B1850-1	T12(P4)	36°10′34.63″N, 100°42′17.73″E	3.73 ± 0.30	11.38 ± 1.00	1.53 ± 0.15	3.56	5.45 ± 0.29	1.75 ± 0.15
10	B1851-2	T13(P4)	36°10′52.18″N, 100°41′45.79″E	2.18 ± 0.20	6.76 ± 0.60	1.54 ± 0.13	3.51	3.56 ± 0.18	1.88 ± 0.15
11	B1852-1	T14(P4)	36°10′55.38″N, 100°41′19.59″E	1.54 ± 0.15	1.54 ± 0.15	1.49 ± 0.15	3.55	3.61 ± 0.18	1.94 ± 0.15
12	B1853-1	T15(P4)	36°11′13.98″N, 100°40′08.40″E	1.54 ± 0.15	1.54 ± 0.15	1.58 ± 0.15	3.34	2.73 ± 0.13	2.01 ± 0.15
13	B1854-1	T16(P4)	36°11′25.79″N, 100°39′54.36″E	1.54 ± 0.15	1.54 ± 0.15	1.59 ± 0.15	3.18	3.57 ± 0.18	2.12 ± 0.15
14	B1855-1	T17(P4)	36°11′32.51″N, 100°38′58.71″E	1.54 ± 0.15	1.54 ± 0.15	1.53 ± 0.15	3.61	2.64 ± 0.13	2.23 ± 0.20
15	B1856-1	T18(P4)	36°12′53.45″N, 100°36′41.91″E	4.00 ± 0.40	12.03 ± 1.20	1.31 ± 0.10	3.14	4.40 ± 0.24	2.31 ± 0.20
16	B1842-1	T19(P4)	36°14′51.18″N, 100°30′52.71″E	2.05 ± 0.20	2.05 ± 0.20	1.33 ± 0.10	3.67	3.17 ± 0.15	2.32 ± 0.20
17	B1842-2	T19(P4)	36°14′51.18″N, 100°30′52.71″E	2.05 ± 0.20	2.05 ± 0.20	1.45 ± 0.14	3.11	4.18 ± 0.21	2.36 ± 0.20
18	B1866-1	T20(P4)	36°6′4.03″N, 100°58′53.48″E	1.14 ± 0.11	1.14 ± 0.11	1.81 ± 0.15	4.21	3.69 ± 0.18	2.47 ± 0.22

As mentioned in the introduction, there are three models regarding the process of Tibetan Plateau uplift: the early uplift, later uplift, and multi-stage uplift models (Xu et al., 1973; Li et al., 1979, 2001; Harrison et al., 1992; Molnar et al., 1993; Coleman and Hodges, 1995; Li and Fang, 1999; Song et al., 2003), of which the multi-stage theory has received the most support (e.g., Li, 1995; Zhong and Ding, 1996; Li and Fang, 1999; Song et al., 2000; Wang et al., 2008, 2012, 2014b; Vandenberghe, 2016). Zhang et al. (2013) proposed that the Tibetan Plateau has experienced five major uplift events at 58–53 Ma, 45–30 Ma, 25–20 Ma, 13–7 Ma, and since 5 Ma. The Guide–Gonghe basin is located on the NE Tibetan Plateau and its uplift history has very important implications for research of the Tibetan Plateau uplift pattern. Research into the regional tectonic evolution and paleostructure of the Tibetan Plateau has shown that the central region (the Qiangtang and Lhasa blocks) had already been uplifted by the late Paleogene. Under the continuous collision of the Indian and Eurasian plates, the Tibetan Plateau expanded, with the Himalayas at the southern end of the plateau being uplifted in the Neogene, and the Qilian Mountains on the northern Plateau uplifted in the late Cenozoic (Wang et al., 2008). Valley incision rates in the eastern Qilian Shan are about 0.09–0.25 mm/yr since 1.4 Ma (Pan et al., 2007). Penecontemporaneous and far-reaching tectonic deformation at about 8 Ma caused the closure of the sedimentary basin and uplift of the mountains on the NE Tibetan Plateau (Song et al., 2000; An et al., 2006; Zhang et al., 2006; Zheng et al., 2006; Lin and Xiao, 2011; Yan et al., 2013). The amount of uplift has been estimated at ~1000–2000 m since 8 Ma from integrated studies of the NE Tibetan Plateau structure and environmental changes that occurred in the late Cenozoic (Harrison et al., 1992; Molnar et al., 1993; Clark et al., 2004). From this, we estimate that the maximum uplift rate of the NE Tibetan Plateau since the Quaternary was ~0.25 mm/yr.

Based on the above, we can summarize that uplift of the Tibetan Plateau has continued since 8 Ma at an average rate of about 0.25 mm/yr, and that the average uplift rate of the NE Tibetan Plateau since the Quaternary has been similar at about 0.26 mm/yr by our results. Therefore, our results support the multi-stage uplift model, which states that the Tibetan Plateau has experienced continuous uplift since 8 Ma. Furthermore, our results do not support the early uplift model, which proposes that uplift of the Tibetan Plateau occurred mainly before the Pliocene, or the late uplift model, which proposes that rapid uplift of the Tibetan Plateau began at 3.6 Ma BP.

6. Conclusions

(1) There are 20 levels of Yellow River terraces in the Gonghe–Guide section of the NE Tibetan Plateau, and the T3–T20 terraces formed at about 0.13, 0.18, 0.23, 0.41, 0.85, 0.93, 1.32, XX, 1.71, 1.75, 1.88, 1.94, 2.01, 2.12, 2.23, 2.31, 2.36, and 2.47 Ma BP, respectively. This suggests that the Yellow River has existed in the Gonghe and Guide basins for the last 2.47 Ma.

(2) The incision rates of the Yellow River in the Gonghe–Guide section indicate that the NE Tibetan Plateau experienced three different stages of uplift. The uplift rates from 2.47–1.71 Ma, 1.71–0.41 Ma, and 0.41 Ma to the present day were about 0.51, 0.09, and 0.35 mm/yr respectively.

(3) The average uplift rate of the NE Tibetan Plateau since the Quaternary has been about 0.26 mm/r. Our results support the multi-stage uplift model, which proposes that the Tibetan Plateau has experienced continuous uplift since 8 Ma. Furthermore, our results do not support the early uplift model, which proposes that uplift of the Tibetan Plateau occurred mainly before the Pliocene, or the late uplift model, which states that rapid uplift of the Tibetan Plateau began at 3.6 Ma.

Table 5
Terrace sequence and ages in the Gonghe–Guide section of the Yellow River.

Terrace level	Height above the Yellow River (m)	Age (Ma)	Terrace level	Height above the Yellow River (m)	Age (Ma)
T1	6–12	0.017	T11	249–258	1.71 ± 0.13
T2	14–20	0.043	T12	284–287	1.75 ± 0.15
T3	27–42	0.134 ± 0.012	T13	324–326	1.88 ± 0.15
T4	48–64	0.176 ± 0.015	T14	327–335	1.94 ± 0.15
T5	80–98	0.228 ± 0.02	T15	381–382	2.01 ± 0.15
T6	125–160	0.41 ± 0.04	T16	396–405	2.12 ± 0.15
T7	165–172	0.82 ± 0.08	T17	420–422	2.23 ± 0.20
T8	186–197	0.93 ± 0.10	T18	446–482	2.31 ± 0.20
T9	210–220	1.32 ± 0.10	T19	503–510	2.36 ± 0.20
T10	236–241	2.20 ± 0.20	T20	643–648	2.47 ± 0.22

Note: The data for terraces T1 and T2 are from Miao et al. (2012).

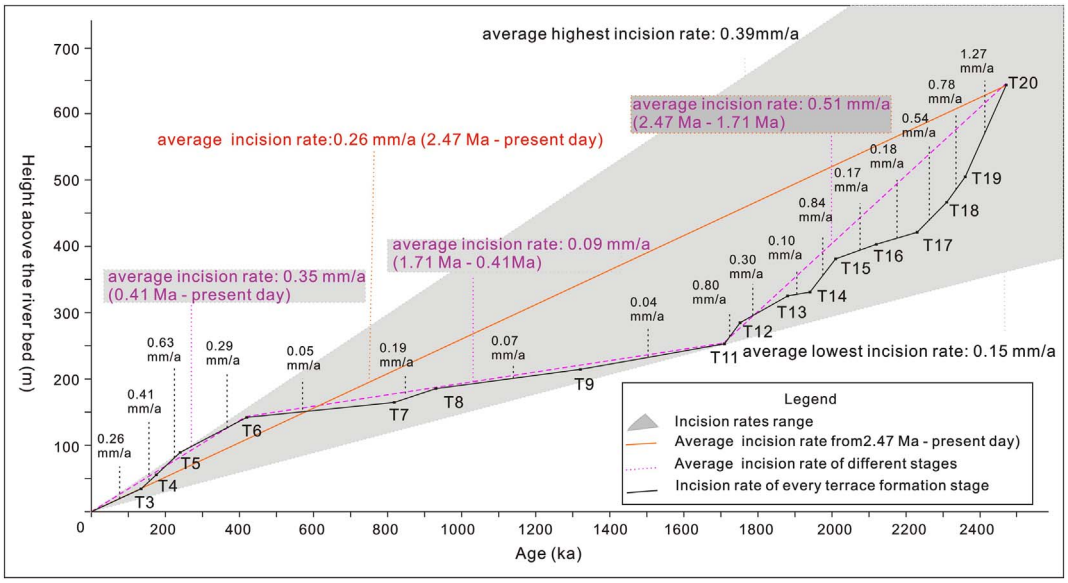

Fig. 10. Evolution of incision rates of the Yellow River in the Gonghe–Guide reach during the Quaternary.

Acknowledgements

The authors thank Professor Jef Vandenberghe, David Bridgland, and 2 anonymous reviewers for their valuable comments and suggestions regarding this manuscript. We also thank Scott Lecce, our editor, for his time and effort dedicated to improving our manuscript. This study was financially supported by the China Geological Survey (grant nos. DD20160269, GZHL20120301, DD20160270 and 12120114042101).

References

Aitken, M.J., 1985. Thermoluminescence Dating. Academic Press, London.
An, Z., Zhang, P., Wang, E., Wang, S., Qiang, X., Li, L., Song, Y., Chang, H., Liu, X., Zhou, W., Liu, W., Cao, J., Li, X., Shen, J., Liu, Y., Ai, L., 2006. Changes of the monsoon-arid environment in China and growth of the Tibetan Plateau since the Miocene. Quaternary Sciences 26 (5), 678–693 (in Chinese with English abstract).
Beerten, K., Stesmans, A., 2007. ESR dating of sedimentary quartz: possibilities and limitations of the single-grain approach. Quat. Geochronol. 2 (1), 373–380.
Beerten, K., Lomax, J., Clémer, K., Stesmans, A., Radtke, U., 2006. On the use of Ti centres for estimating burial ages of Pleistocene sedimentary quartz: multiple-grain data from Australia. Quat. Geochronol. 1 (2), 151–158.
Blackwell, B.A.B., Skinner, A.R., Blickstein, J.I.B., Montoya, A.C., Florentin, J.A., Baboumian, S.M., et al., 2016. ESR in the 21st century: from buried valleys and deserts to the deep ocean and tectonic uplift. Earth Sci. Rev. 158, 125–159.
Bridgland, D.R., 2000. River terrace systems in north–west Europe: an archive of environmental change, uplift and early human occupation. Quat. Sci. Rev. 19, 1293–1303.
Bridgland, D.R., Westaway, R., 2008. Climatically controlled river terrace staircases: a worldwide Quaternary phenomenon. Geomorphology 98, 285–315.
Bridgland, D.R., Maddy, D., Bates, M., 2004. River terrace sequences: templates for Quaternary geochronology and marine–terrestrial correlation. J. Quat. Sci. 19, 203–218.
Buylaert, J.P., Vandenberghe, D., Murray, A.S., Huot, S., De Corte, F., Van den Haute, P., 2007. Luminescence dating of old (N70 ka) Chinese loess: a comparison of single-aliquot OSL and IRSL techniques. Quat. Geochronol. 2, 9–14.
Buylaert, J.P., Murray, A.S., Vandenberghe, D., Vriend, M., De Corte, F., Van den Haute, P., 2008. Optical dating of Chinese loess using sand-sized quartz: establishing a time frame for Late Pleistocene climate changes in the western part of the Chinese Loess Plateau. Quat. Geochronol. 3, 99–113.
Chen, J., Liang, X., Feng, J., Tuo, X., 1991. A study of annealing on e'center in quartz. Journal of Sichuan University 28, 314–317 (in Chinese with English abstract).
Clark, M.K., Schoenbohm, L.M., Royden, L.H., Whipple, K.X., Burchfiel, B.C., Zhang, X., Tang, W., Wang, E., Chen, L., 2004. Surface uplift, tectonics, and erosion of eastern Tibet from large-scale drainage patterns. Tectonics 23 (1), TC1006.
Coleman, M., Hodges, K., 1995. Evidence for Tibetan plateau uplift before 14 myr ago from a new minimum age for east west extension. Nature 374 (6517), 49–52.
Dai, S., Fang, X., Dupont-Nivet, G., Song, C., Gao, J., Krijgsman, W., Langereis, C., Zhang, W., 2006. Magnetostratigraphy of Cenozoic sediments from the Xining basin: tectonic implications for the northeastern Tibetan Plateau. J. Geophys. Res. Atmos. 111 (B11), 335–360.
Fothergill, P.A., Ma, H., 1999. Preliminary observations on the geomorphic evolution of the guide basin, Qinghai province, China: implications for the uplift of the northeast margin of the Tibetan Plateau. Geol. Soc. Lond. Spec. Publ. 162 (1), 183–200.
Gao, J.C., Liang, X.Z., 1995. Dating of α-quartz by determining E′ centre concentration. Nucl. Technol. 18, 499–508 (in Chinese with English abstract).
Grün, R., 1989a. ESR dating for the early Earth. Nature 338, 543–544.
Grün, R., 1989b. Electron spin resonance (ESR) dating. Quat. Int. 1, 65–109.
Harrison, T.M., Copeland, P., Kidd, W.S., Yin, A., 1992. Raising Tibet. Science 255 (5052), 1663–1670.
He, Z.X., Zhang, X.J., Jia, L.Y., Wu, F.D., Zhou, Y.Q., Bao, S.Y., Bao, Z.Q., Yin, Z.G., Guo, B., 2014. Genesis of piedmont terraces and its Neotectonic Movement significance in Langshan Mountain area, Inner Mongolia. Geoscience 28 (1), 98–108 (in Chinese with English abstract).
He, Z.X., Zhang, X.J., Qiao, Y., Bao, S., Lu, C.Y., He, X.L., 2015. Formation of the Yalong downstream terraces in the SE Tibetan Plateau and its implication for the uplift of the plateau. Acta Geol. Sin. 89 (2), 542–560.
Herfried, M., Frank, P., Olivier, F., 2012. Climatic and tectonic controls on the

development of the River Ognon terrace system (eastern France). Geomorphology 151-152 (1), 126–138.
Hu, Z.B., Pan, B.T., Wang, J.P., Cao, B., Gao, H.S., 2012. Fluvial terrace formation in the eastern Fenwei Basin, China, during the past 1.2 Ma as a combined archive of tectonics and climate change. J. Asian Earth Sci. 60, 235–245.
Huang, P.H., 1994. Study on electron spin resonance (ESR) dating of fault movement. Seismol. Geol. 16 (3), 269–274 (in Chinese with English abstract).
Jia, L., 2015. Neotectonics and Geomorphic Response in Western Yin Mountains Area, Inner Mongolia, Northern China. China University of Geosciences for Doctoral Degree (in Chinese with English abstract).
Jia, L., Zhang, X., He, Z., He, X., Wu, F., Zhou, Y., Fu, L., Zhao, J., 2015. Late Quaternary climatic and tectonic mechanisms driving river terrace development in an area of mountain uplift: a case study in the Langshan area, Inner Mongolia, northern China. Geomorphology 234, 109–121.
Jia, L., Zhang, X., Ye, P., Zhao, X., He, Z., He, X., Zhou, Q.S., Li, Jie, Ye, M.N., Wang, Z., Meng, J., 2016. Development of the alluvial and lacustrine terraces on the northern margin of the Hetao Basin, Inner Mongolia, China: implications for the evolution of the Yellow River in the Hetao area since the late Pleistocene. Geomorphology 263, 87–98.
Laurent, M., Falguères, C., Bahain, J.J., Rousseau, L., Van Vliet Lanoé, B., 1998. ESR dating of quartz extracted from Quaternary and Neogene sediments: method, potential and actual limits. Quat. Sci. Rev. 17, 1057–1062.
Li, J., 1995. Uplift of Qinghai-Xizang (Tibet) Plateau and Global Change. Lanzhou University Press, Lanzhou 207 p. (in Chinese).
Li, J., Fang, X., 1999. The uplift of Tibetan Plateau and environment changes. Chin. Sci. Bull. 44 (23), 2117–2124.
Li, J., Wen, S.X., Zhang, Q.S., Wang, F.B., Zheng, B.X., Li, B.Y., 1979. Discussion on the age, amplitude and form of the uplifting of the Qinghai-Tibetan Plateau. Science China 6, 88–102 (in Chinese).
Li, J., Fang, X.M., Pan, B.T., Zhao, Z.J., Song, Y.G., 2001. Late Cenozoic intensive uplift of Qinghai-Xizang Plateau and its impacts on environments in surrounding area. Quaternary Sciences 21 (05), 381–391 (in Chinese with English abstract).
Liang, X.Z., 1990. Electron spin resonance dating method principle and its application in geology. New Development of Science and Technology 4, 55–58 (in Chinese).
Liang, X.Z., 1993. A study on resetting for E′ centre dating of α-quartz. Nucl. Tech. 16 (4), 213–216 (in Chinese with English abstract).
Liang, X.Z., Gao, J.C., 1999. Study on the α-quartz dating of fault-related ore mineralization. J. Mineral. Petrol. 19, 69–71 (in Chinese with English abstract).
Lin, X., Xiao, J., 2011. The uplift history of the Haiyuan-Liupan Shan region northeast of the present Tibetan Plateau: integrated constraint from stratigraphy and thermochronology. J. Geol. 119 (4), 372–393.
Liu, C., Yin, G., Gao, L., Han, F., Zhang, H., 2011. Research advances in ESR geochronology of Quaternary deposits. Dizhen Dizhi 33 (2), 490–498 (in Chinese with English abstract).
Lu, H.Y., An, Z.S., Wang, X.Y., Tan, H.B., Zhu, R.X., Ma, H.Z., Li, Z., Miao, X.D., Wang, X.Y., 2004. Geomorphologic evidence of phased uplift of the northeastern Qinghai-Tibet Plateau since 14 million years ago. Science in China 47 (9), 822–833.
Maddy, D., Bridgland, D.R., Green, C.P., 2000. Crustal uplift in southern England: evidence from the river terrace records. Geomorphology 33, 167–181.
Maddy, D., Bridgland, D.R., Westaway, R., 2001a. Uplift-driven valley incision and climate controlled river terrace development in the Thames Valley, UK. Quat. Int. 79, 23–36.
Maddy, D., Macklin, M.G., Woodward, J.C., 2001b. River Basin Sediment Systems: Archives of Environmental Change. Balkema, Lisse (503 pp).
Maddy, D., Demir, T., Bridgland, D.R., Veldkamp, A., Stemerdink, C., van der Schriek, T., Westaway, R., 2008. The Early Pleistocene development of the Gediz River, Western Turkey: an uplift-driven, climate-controlled system? Quat. Int. 189, 11–128.
Martins, A.A., Cunha, P.P., Huot, S., Murray, A.S., Buylaert, J.P., 2009. Geomorphological correlation of the tectonically displaced Tejo River terraces (Gavião-Chamusca area, central Portugal) supported by luminescence dating. Quat. Int. 199, 75–91.
Merritts, D.J., Vincent, K.R., Wohl, E.E., 1994. Long river profiles, tectonism, and eustasy: a guide to interpreting fluvial terraces. J. Geophys. Res. 99, 14031–14050.
Miao, Q., Li, L.S., Qian, F., Zhao, Z., 2012. Study on the terraces and neotectonics of the Yellow River in guide area, Qinghai province. Geology and Resources 5, 493–496 (in Chinese with English abstract).
Molnar, P., Tapponnier, P., 1975. Cenozoic tectonics of Asia: effects o f a continental collision. Science 189, 419–426.
Molnar, P., England, P., Martinod, J., 1993. Mantle dynamics, uplift of the Tibetan Plateau, and the Indian monsoon. Rev. Geophys. 31 (31), 357–396.
Nie, J., Song, C., Fang, X., Xianhai, X.U., Sun, D., 2003. Paleomagnetic constraint on appearance of the yellow river in the guide basin in the NE Tibetan Plateau and its geomorphologic implications. Mar. Geol. Quat. Geol. 23 (2), 59–64.
Pan, B., Gao, H., Wu, G., Li, J., Li, B., Ye, Y., 2007. Dating of erosion surface and terraces in the eastern Qilian Shan, northwest China. Earth Surf. Process. Landf. 32, 143–154.
Pan, B., Su, H., Hu, Z., Hu, X., Gao, H., Li, J., Kirby, E., 2009. Evaluating the role of climate and tectonics during non-steady incision of the Yellow River: evidence from a 1.24 Ma terrace record near Lanzhou, China. Quat. Sci. Rev. 28 (27), 3281–3290.
Patriat, P., Achache, J., 1984. India-Eurasia collision chronology has implications for crustal shortening and driving mechanism of plates. Nature 311, 615–621.
Perrineau, A., Woerd, J.V.D., Gaudemer, Y., Liuzeng, J., Pik, R., Tapponnier, P., Thuizat, R., Zheng, R.Z., 2011. Incision rate of the Yellow River in northeastern Tibet constrained by ^{10}Be and ^{26}Al cosmogenic isotope dating of fluvial terraces: implications for catchment evolution and plateau building. Geol. Soc. Lond. Spec. Publ. 353, 189–219.
Ren, J.J., Zhang, S.M., Meigs, A.J., Yeats, R.S., Rui, D., Shen, X.M., 2014. Tectonic controls for transverse drainage and timing of the Xin-Ding paleolake breach in the upper reach of the Hutuo River, north China. Geomorphology 206, 452–467.
Ren, S., Song, C., Li, J., 2016. Application of electron spin resonance (ESR) dating to ductile shearing: examples from the Qinling orogenic belt, China. J. Struct. Geol. 85, 12–17.
Rink, W.J., Bartoll, J., Schwarcz, H.P., Shane, P., Bar-Yosef, O., 2007. Testing the reliability of ESR dating of optically exposed buried quartz sediments. Radiat. Meas. 42 (10), 1618–1626.
Royden, L.H., Burchfiel, B.C., van der Hilst, R.D., 2008. The geological evolution of the Tibetan Plateau. Science 321, 1054–1058.
Shen, C.B., Mei, L.F., Tang, J.G., Wu, M., 2008. Geochronology evidences for tectonic deformation of Dabashan Fold-thrust Belt in Central China. Atomic Energy Science and Technology 42, 574–576 (in Chinese with English abstract).
Song, Y., Fang, X., Li, J., An, Z., Yang, D., Lu, L., 2000. Age of red clay at Chaona section near eastern Liupan Mountain and its tectonic significance. Quat. Res. 20, 457–463 (in Chinese with English abstract).
Song, C., Fang, X., Gao, J., Nie, J., Yan, M., Xu, X., 2003. Magnetostratigraphy of late Cenozoic fossil mammals in the Northeastern margin of the Tibetan Plateau. Chin. Sci. Bull. 48 (2), 188–193.
Sun, Y.G., Fang, H.B., Zhang, K., Zhao, F.Y., Liu, S.Y., 2007. Step-like landform system of the Gonghe Basin and the uplift of the Qinghai-Tibet Plateau and development of the Yellow River. Geol. China 34 (6), 1141–1147 (in Chinese with English abstract).
Tapponnier, P., Zhiqin, X., Roger, F., Meyer, B., Arnaud, N., Wittlinger, G., Jingsui, Y., 2001. Oblique stepwise rise and growth of the Tibet Plateau. Science 294 (5547), 1671–1677.
Vandenberghe, J., 1995. Timescale, climate and river development. Quat. Sci. Rev. 14, 631–638.
Vandenberghe, J., 2002. The relation between climate and river processes, land-forms and deposits during the Quaternary. Quat. Int. 91, 17–23.
Vandenberghe, J., 2003. Climate forcing of fluvial system development: an evolution of ideas. Quat. Sci. Rev. 22, 2053–2060.
Vandenberghe, J., 2015. River terraces as a response to climatic forcing: formation processes, sedimentary characteristics and sites for human occupation. Quat. Int. 370, 3–11.
Vandenberghe, J., 2016. From planation surfaces to river valleys. Bulletin de la Société Géographique de Liège 67, 93–106.
Vandenberghe, J., Maddy, D., 2001. The response of river systems to climate change. Quat. Int. 79, 1–3.
Vandenberghe, J., Wang, X., Lu, H., 2011. Differential impact of small-scaled tectonic movements on fluvial morphology and sedimentology (the Huang Shui catchment, NE Tibet Plateau). Geomorphology 134, 171–185.
Viveen, W., Schoorl, J.M., Veldkamp, A., van Balen, R.T., Desprat, S., Vidal-Romani, J.R., 2013. Reconstructing the interacting effects of base level, climate, and tectonic uplift in the lower Miño River terrace record: a gradient modelling evaluation. Geomorphology 186, 96–118.
Wang, C., Zhao, X., Liu, Z., Lippert, P.C., Graham, S.A., Coe, R.S., Yi, H., Zhu, L., Liu, S., Li, Y., 2008. Constraints on early uplift history of the Tibetan Plateau. Proc. Natl. Acad. Sci. 105 (13), 4987.
Wang, P., Jiang, H.C., Yuan, D.Y., Liu, X.W., Zhang, B., 2010. Optically stimulated luminescence dating of sediments from the Yellow River terraces in Lanzhou: tectonic and climatic implications. Quat. Geochronol. 5, 181–186.
Wang, X., Lu, H., Vandenberghe, J., Zheng, S., van Balen, R.T., 2012. Late Miocene uplift of the NE Tibetan Plateau inferred from basin filling, planation and fluvial terraces in the Huang Shui catchment. Glob. Planet. Chang. 88-89, 10–19.
Wang, C., Dai, J., Zhao, X., Li, Y., Graham, S.A., He, D., Bo, R., Meng, J., 2014a. Outward-growth of the Tibetan Plateau during the Cenozoic: a review. Tectonophysics 621, 1–43.
Wang, X., Van Balen, R., Yi, S., Vandenberghe, J., Lu, H., 2014b. Differential tectonic movements in the confluence area of the Huang Shui and Huang He rivers (Yellow River), NE Tibetan Plateau, as inferred from fluvial terrace positions. Boreas 43, 469–484.
Westaway, R., 2009. Active crustal deformation beyond the SE margin of the Tibetan Plateau: constraints from the evolution of fluvial systems. Glob. Planet. Chang. 68, 395–417.
Whipple, K.X., Kirby, E., Brocklehurst, S.H., 1999. Geomorphic limits to climate induced increases in topographic relief. Nature 401, 39–43.
Xu, R., Tao, J.R., Sun, X.J., 1973. Finding the fossil group of Oakson Mountain Xxiabangma and its significance in botany and stratigraphy. J. Integr. Plant Biol. 15 (1), 103–119 (in Chinese).
Xu, S.Y., Xu, D.F., Sha, S.R., 1984. A discussion on the development of landforms and evolution of environments in the Gonghe Basin. Journal of Lanzhou University 20 (1), 146–157 (in Chinese with English abstract).
Yan, M., Fang, X., Van, D.V.R., Song, C., Li, J., 2013. Neogene rotations in the Jiuquan Basin, Hexi corridor, China. Geol. Soc. Lond. Spec. Publ 373 p. (in Chinese with English abstract).
Yang, D., Wang, Y., 1996. On river terraces of the upper reaches of the Huanghe River and change of the river system. Sci. Geogr. Sin. 2, 137–148 (in Chinese with English abstract).
Yang, K.G., Liang, X.Z., Xie, J.L., Yang, K.F., 2006. ESR dating, the principle and application of a method to determine active ages of brittle faults. Adv. Earth Science 21 (4), 430–435 (in Chinese with English abstract).
Zhang, P., Zheng, D.W., Yin, G.M., Yan, D.Y., Zhang, G.L., Li, C.Y., Wang, Z.C., 2006. Discussion on late Cenozoic growth and rise of northeastern margin of the Tibetan Plateau. Quaternary Sciences 26 (1), 5–13 (in Chinese with English abstract).
Zhang, K.X., Wang, G.C., Cao, K., Liu, C., Xiang, S.Y., Hong, H.L., Kou, X.H., Xu, Y.D., Chen, F.N., Meng, Y.N., Chen, R.M., 2008. Cenozoic sedimentary records and geochronological constraints of differential uplift of the Qinghai-Tibet Plateau. Science in

China 51 (11), 1658–1672.
Zhang, K.X., Wang, G.C., Ji, J.L., Luo, M.S., Kou, X.H., Wang, Y.M., Xu, Y.D., Chen, F.N., Chen, R.M., Song, B.W., Zhang, J.Y., Liang, Y.P., 2010. Paleogene-Neogene stratigraphic realm and sedimentary sequence of the Qinghai-Tibet Plateau and their response to uplift of the plateau. Science China 53 (9), 1271–1294.
Zhang, K., Wang, G., Yadong, X.U., Luo, M., Junliang, J.I., Xiao, G., et al., 2013. Sedimentary evolution of the Qinghai-Tibet Plateau in Cenozoic and its response to the uplift of the plateau. Acta Geol. Sin. 87 (2), 555–575.
Zhao, Z., Liu, B., 2005. The primary perspective of longyang gorge formation. Northwest. Geol. 38 (2), 24–32 (in Chinese with English abstract).
Zheng, D., Zhang, P.Z., Wan, J., Yuan, D., Li, C., Yin, G., Zhang, G., Wang, Z., Min, W., Chen, J., 2006. Rapid exhumation at ~8 Ma on the Liupan Shan thrust fault from apatite fission-track thermochronology: implications for growth of the northeastern Tibetan Plateau margin. Earth Planet. Sci. Lett. 248 (1–2), 198–208.
Zhong, D.L., Ding, L., 1996. Rising process of the Qinghai-Xizang (Tibet) Plateau and its mechanism. Sci. China Ser. D Earth Sci. 39 (4), 369–379 (in Chinese).
Zhong, K., Liang, X., Liu, Z., Shu, L., Fanyou, L.I., Shi, Y., Tang, J., 2004. Heat-activated ESR dating of α quartz and Cenozoic tectonic events in the Yunnan segment of the Sanjiang tectonic zone, eastern Tibet. Regional Geology of China 23 (12), 1231–1237 (in Chinese with English abstract).
Zhu, Q.B., Yang, K.G., Cheng, W.Q., 2011. Structural evolution of northern Jiangnan uplift: evidence from ESR dating. Geoscience 25, 31–38 (in Chinese with English abstract).